Chinese Chemical Letters 34 (2023) 107929

Contents lists available at ScienceDirect

Chinese Chemical Letters

journal homepage: www.elsevier.com/locate/cclet

Agar-derived nitrogen-doped porous carbon as anode for construction of cost-effective lithium-ion batteries

Tong Wang[a,b], Jingquan Sha[b,*], Wenwen Wang[b], Yuhan Ji[b], Zhi-Ming Zhang[a,*]

[a] Institute for New Energy Materials & Low Carbon Technologies, School of Chemistry and Chemical Engineering, Tianjin University of Technology, Tianjin 300384, China
[b] School of Chemistry, Chemical Engineering and Materials, Jining University, Qufu 273100, China

ARTICLE INFO

Article history:
Received 18 September 2022
Revised 13 October 2022
Accepted 19 October 2022
Available online 22 October 2022

Keywords:
Agar
Porous carbon
N-doping
Anode
Lithium-ion battery

ABSTRACT

Balancing cost and performance of porous carbon (PC) as anode for lithium-ion battery (LIBs) is the key to effectively promote commercial application. Herein, low-cost N-doped PC (NPC-Ts, $T = 600$, 750 and 900 °C) were facilely prepared in batches *via* one-pot pyrolysis of agar with different carbonization temperature. The NPC-750 with specific surface area of 2914 m^2/g and N content of 2.84% exhibits an ultrahigh reversible capacity of 1019 mAh/g at 0.1 A/g after 100 cycles and 837 mAh/g at 1 A/g after 500 cycles. Remarkably, the resulting LIBs exhibit an ultrafast charge-discharge feature with a remarkable capacity of 281 mAh/g at 10 A/g and a superlong cycle life with a capacity retention of 87% after 5000 cycles at 10 A/g. Coupling with $LiFePO_4$ cathode, the fabricated lithium-ion full cells possess high capacity, excellent rate and cycling performances (125 mAh/g at 100 mA/g, capacity retention of 95%, after 220 cycles), highlighting the practicability of this NPC-750 as the anode materials.

Lithium-ion battery (LIBs) are regarded as one of the most promising large-scale energy storage device due to the excellent stability, no memory effect and large energy density [1–3]. It was believed that the nature of electrode materials have played an important role in governing and improving the performance of LIBs. In this field, the conventional graphite-based anodes usually exhibit low specific capacity (theoretical capacity 372 mAh/g) and unfavorable rate capability, limiting the broad application of LIBs [4–6]. As a result, many noncarbon anode materials (metal compounds- oxides [7,8], sulfides [9], carbides [10], tin [11], silicon [12], and others [13]) and carbonaceous materials (graphene [14], carbon nanotubes [15], fullerene [16], carbon fiber [17] and others [18,19]) were explored and expected to replace graphite for reaching better LIBs performance. Balancing the specific capacity and process cost, carbon materials were still regarded as the most commercially valued anode material for LIBs.

Porous carbon (PC) as a typical amorphous carbon material, has great potential to act as commercial anode for LIBs, due to its high cost-performance and environmental friendliness [20,21]. To date, fossil fuels, polymers and biomass-based materials were widely used as precursors to prepare PC (Scheme 1), which exhibited promising specific capacities in the range of 300–800 mAh/g at 0.1 C (1 C = 372 mA/g) [22,23]. Moreover, the heteroatom-doping, especially N-doping, could enhance the charge mobility and wettability of PC, and generate more Li^+ adsorption-sites and more pseudo-capacitance deeds to further increase electrochemical performance [24], especially at large currents. To the best our knowledge, the fabrication of heteroatom-doped PC has been achieved by template method and *in situ*-pyrolysis (including physical and chemical activation) [25,26], but high process cost with hugely energy-consuming process further limited their real commercial application. In this field, more and more efforts mainly focus on balancing the cost and performance of PC anodes for LIBs to promote commercial application.

Herein, the low-cost agar as sustainable precursor, urea as N source, and KOH as activator were employed for batch preparation of a series of N-doped PC (NPC-Ts, $T = 600$, 750 and 900 °C) with different temperature *via* a facile one-pot pyrolysis due to the following advantages: (1) Agar, an abundant, inexpensive, carbon-rich polysaccharide derived from seaweed, is easy to cross-link into 3D porous hydrogels through hydrogen bonds to facilitate encapsulation of water-soluble activator (KOH) and the N source spices (urea) [27,28]. (2) Doped N configuration (pyridinic-N, pyrrolic-N, or graphitic-N) in PC can play an important role in Li^+ storage [29,30]. (3) Carbonization temperature is also one of crucial factors to the activity of the activator and morphology as well as ele-

* Corresponding authors.
E-mail addresses: Shajq@jnxy.edu.cn (J. Sha), zmzhang@email.tjut.edu.cn (Z.-M. Zhang).

https://doi.org/10.1016/j.cclet.2022.107929
1001-8417/

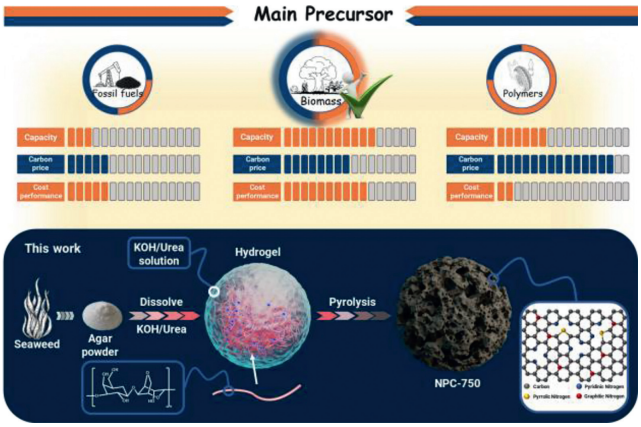

Scheme 1. Comparison of main properties of three main precursors for PC-based anode materials of LIBs (top). Schematic illustration of the synthesis route for NPC in this work (bottom).

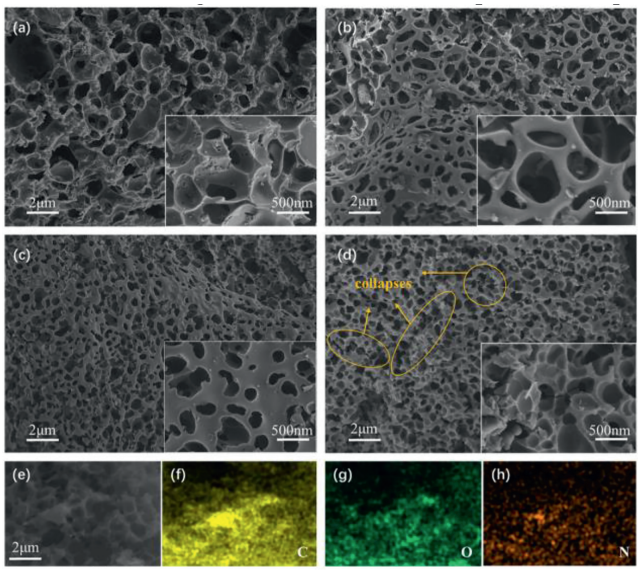

Fig. 1. SEM images of (a) PC-750, (b) NPC-750, (c) NPC-600, (d) NPC-900. (e-h) SEM image of NPC-750 and the mapping analysis of elemental carbon, nitrogen and oxygen in NPC-750 architecture.

ments content of resulting PC [26,28]. As a consequence, the NPC-750 achieves the best electrochemical performances among these NPC-Ts anode materials of LIBs with ultrahigh reversible capacity of 1019 mAh/g at 0.1 A/g after 100 cycles and 837 mAh/g at 1 A/g after 500 cycles. LIB with NPC-750 as the anode materials exhibit ultrafast charge-discharge feature with 281 mAh/g capacity at 10 A/g, and a superlong cycle life with a capacity retention of 87% after 5000 cycles at 10 A/g. These performances and practicality of NPC-750 were much superior to that of most biomass-derived carbon materials and graphene/carbon-based materials (Table S4 in Supporting information). Coupling with $LiFePO_4$ cathode, the fabricated Li-ion full cells possess of exhibit high capacity, excellent rate capability and cycling performances (125 mAh/g, capacity retention of 95% after 220 cycles), highlighting the practicability of NPC-750 as a promising LIB anode.

The synthesis of NPC-750 is shown at the bottom of Scheme 1. Briefly, the agar, KOH, and urea are dissolved in deionized water, and the mixture was heated to form 3D hydrogels. At last, the obtained product is pyrolyzed at 750 °C, and the as-synthesized material was named NPC-750 (the detail experiments are provided in the supporting information). As shown in Fig. 1 and Figs. S1–S4 (Supporting information), scanning electron microscope (SEM) images of NPC-Ts and the control sample of PC-750 all exhibit a 3D interconnected network with micrometer-scale pore resulting by the KOH etching, which was beneficial for the fast Li^+ transportation between the electrolyte and carbon materials. Specifically, PC-750 is made up of micrometer or sub-micrometer hollow spheres with thick carbon wall (Fig. 1a). Compared with PC-750, NPC-750 behaves closer to a 3D network structure with the thinner carbon wall and higher porosity (Fig. 1b), attributed to the etching action of urea. Moreover, NPC-600 (Fig. 1c) exhibits similar shape to that of NPC-750 with a lower porosity due to weaker etching effect of activator (KOH) at low calcination temperature. However, the pore shape of NPC-900 (Fig. 1d) is closer to that of PC-750 not NPC-750, resulting by the ubiquitous collapse of pores or excessive etching at a higher calcination temperature. Furthermore, elemental mapping of NPC-750 (Figs. 1e-h) shows well-distribution of carbon, nitrogen and oxygen elements, indicating the successful doping N in NPC-750. Powder X-ray diffraction (PXRD) patterns of PC-750 and NPC-Ts all exhibit the same diffraction pattern (Fig. S5a in Supporting information). More specifically, a dominant broad diffraction peak near 23.6° and an inconspicuous peak near 43° were observed for the (002) and (100) crystal plane of carbon, respectively, indicating that the formation of amorphous carbon during destroying carbon structure in agar [31]. According to Bragg's law, the average *d* spacing for (002) planes of PC-750 and NPC-Ts is close to *ca.* 0.376 nm (0.335 nm for graphite), which is conducive to boost the Li^+ intercalation. Note that there was no significant difference in diffraction pattern for the PC-750 and NPC-Ts, indicating no effect of calcination temperature on their amorphous nature. As well known, highly defects and disordered degree of carbon are conducive to providing more active sites for the Li^+ intercalation [29], which can be evaluated from peak intensity ratio of D-band and G-band (I_D/I_G) of Raman spectra. As shown in Fig. S5b (Supporting information), two peaks at 1333 cm^{-1} (D band) and 1559 cm^{-1} (G band) can be observed in all materials. Among the NPC-750 shows a higher peak intensity ratio ($I_D/I_G = 0.96$) than PC-750 (0.82), NPC-600 (0.84), and NPC-900 (0.88), indicating more defects induced by N doping and KOH etching. To confirm this result, N_2 adsorption-desorption isotherms were measured to further explore the porous structure. As shown in Figs. S5c and d (Supporting information), there is a sharp adsorption capacity increase in the low- and the high-pressure region for NPC-750, confirming the presence of micropores and macropores, and a hysteresis loops in medium-pressure region without obvious saturation adsorption platform indicates the presence of extremely irregular mesoporous. In comparison, there is not the sharp increase of adsorption in the high-pressure region for NPC-600 and NPC-900, indicating the disappearance of the macropores in these two materials. Moreover, PC-750 and NPC-Ts all exhibit large specific surface areas (SSA) and pore volume (Table S1 in Supporting information). Compared to PC-750 (1753 m^2/g, 1.5456 mL/g, 3.5268 nm), the NPC-750 has larger specific surface areas and pore volume (2914 m^2/g, 2.3479 mL/g) and smaller average pore size (3.2224 nm) due to the rich microporous structure from the edge defects induced by N doping. Among these samples, NPC-600 has the smallest specific surface areas (675 m^2/g) and pore volume (0.4401 mL/g), and NPC-900 achieves staggering specific surface areas of 3992 m^2/g with the pore volume of 3.0531 mL/g. All these results can be explained preliminarily: (1) With a lower calcination temperature ($T < 700$ °C), the KOH activator exhibits weaker etching ability, resulting in thicker carbon wall, lower SSA and disorder, smaller porosity. (2) As the increase of temperature, the strong etching activity of KOH can induce more defects, higher SSA and the emergence of macropores in NPC. (3) When the temperature continues to rise ($T > 800$ °C), the etching activity of KOH continues to increase, and the volatilization of gas

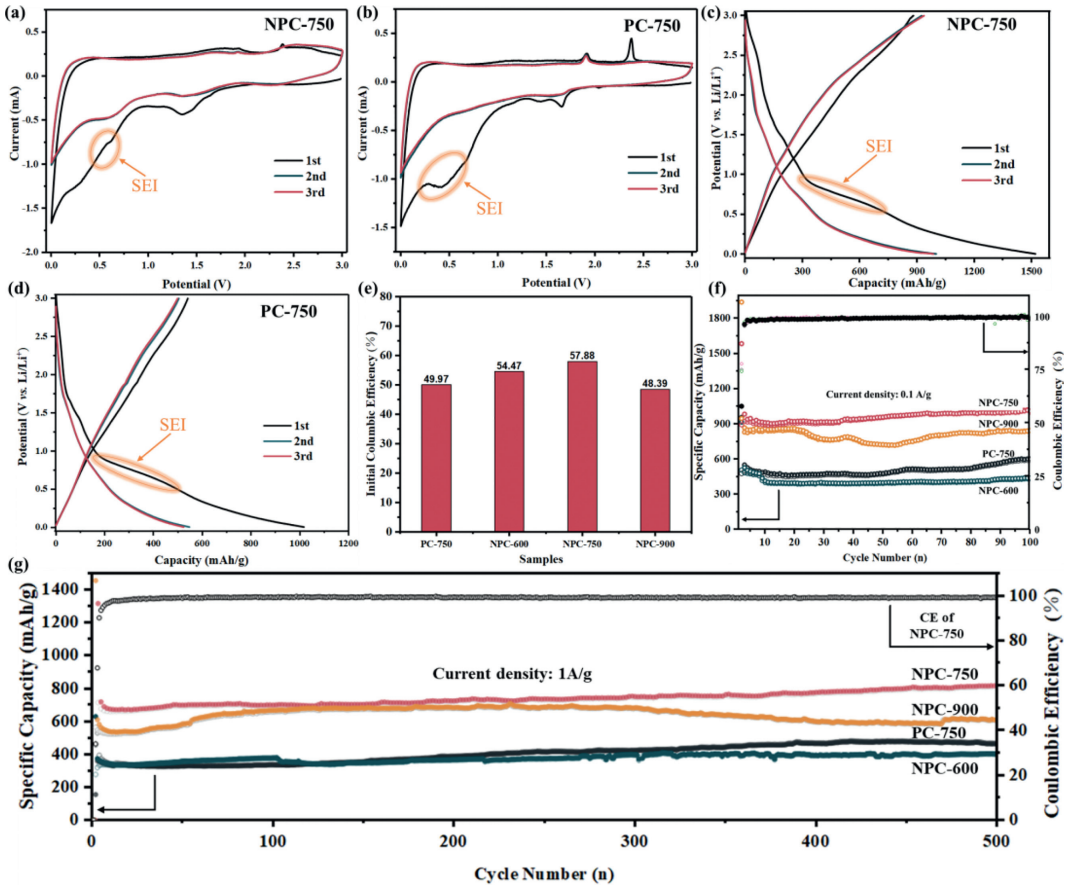

Fig. 2. (a, b) The first three cycles of the CV curves for NPC-750 and PC-750. (c, d) The first three cycles of the charge and discharge curves of NPC-750 and PC-750. (e) The ICE of PC-750 and NPC-Ts at 0.1 A/g. (f) Stability test of the PC-750 and NPC-T for 100 cycles at 0.1 A/g. (g) Stability test of the PC-750 and NPC-Ts for 500 cycles at 1 A/g.

containing N and excessive etching effect results in the collapse of macropores.

To explore the electrochemical properties of anode materials NPC-Ts for LIBs, the cyclic voltammogram (CV) ranging from 0.01 V to 3.0 V *versus* Li/Li^+ at a scan rate of 0.5 mV/s were performed. Due to similar CV curves of all the NPC-Ts (Figs. 2a and b, Fig. S6 in Supporting information), NPC-750 were selected as the typical for further discussion. More specifically, NPC-750 and PC-750 both display an observed peak at ~0.6 V at the first cathodic scan, attributed to the formation of solid electrolyte interphase (SEI). The protuberant reduction peaks at ~1.3 V for the NPC-750 and at ~1.6 V and ~1.4 V for PC-750 were observed, then disappeared at the subsequent cycles, which can be assigned to the irreversible insertion of Li^+ into the interfacial storage sites [32]. For the first anodic scan, NPC-750 and PC-750 both show two protuberant oxidation peaks at ~1.91 V and ~2.37 V, corresponding to Li^+ extraction. In the subsequent cycles, the oxidation peak at 2.3 V disappear, denoting the end of the side reaction [33]. After that, CV curves were almost overlapped, indicating the stable and superior reversibility of NPC-Ts as anode for LIBs. Moreover, the dis-/charge profiles of the first three cycles were explored at 0.1 A/g. As shown in Figs. 2c and d and Fig. S7 (Supporting information), a plateau below 1.0 V in the first discharge was attributed to the formation of SEI for PC-750 and NPC-Ts, and no obvious voltage plateaus were observed during the following dis-/charge process, a typical feature of the carbonaceous materials [34]. The initial discharge and charge capacities of NPC-750 are 1619 and 938 mAh/g, respectively, and the initial columbic efficiency (CE) is 57.9%, which is highest among PC-750 and other NPC-Ts (Fig. 2e and Table S2 in Supporting information). This result can be explained as follows: (1) Compared with PC-750 and NPC-600, higher SSA and more porosity of NPC-750 could provide an electrolyte-electrode contact interface and give rise to initial Li^+ intercalation. (2) Compared with NPC-900, overlarge SSA and porosity could loss more irreversible capacity to form SEI and give adverse effect for Li^+ intercalation. After 100 cycles, the NPC-750 still remains the highest reversibly capacities of 1019 mAh/g, higher than that of NPC-900 (820 mAh/g), NPC-600 (443 mAh/g) and PC-750 (603 mAh/g) (Fig. 2f). To further evaluate the cycle stability of NPC-Ts and PC-750, the dis-/charge performances were evaluated at constant 1 A/g (Fig. 2g). The initial reversibly capacity of PC-750, NPC-600, NPC-750 and NPC-900 is 360.1, 374.7, 714.2 and 564.2 mAh/g, respectively. After 500 cycles, the specific capacity maintains at 464, 401, 837 and 607 mAh/g, respectively, and CE can reach above 99%, indicating their commendable cycling stabilities. Noticeably, both NPC-750 and PC-750 display a slight but continuous increase of the capacity after *ca.* 200 cycles, maybe attributed to the delayed wetting of the electrolytes into the N-doped PC [34]. Moreover, the reversible formation/decomposition process of angel-like film on the interface of PC also provided amounts of interfacial storage sites for excess Li^+ through the "pseudo-capacitance" behavior [34].

As we all know, doped N configuration (pyridinic-N, pyrrolic-N or graphitic-N) in PC plays an important role in the Li^+ storage process [29]. As to the net energy change, pyridinic N (−0.28 eV) was lower than those of graphitic N (0.07 eV) and pyrrolic N (14.94 eV), leading to the highest activity for association of Li atoms (Fig. S8a in Supporting information) [34]. This reason encourages us to further measure the content of doped N configuration by X-ray photoelectron spectroscopy (XPS, Fig. S8b in Supporting information), in order to understand the best Li^+ storage

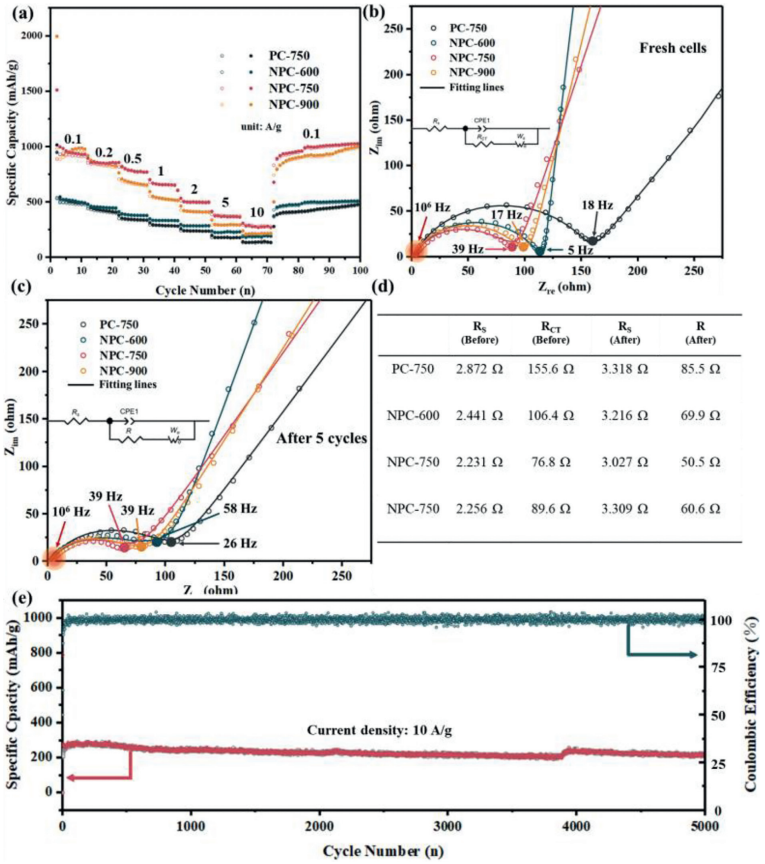

	R_s (Before)	R_{CT} (Before)	R_s (After)	R (After)
PC-750	2.872 Ω	155.6 Ω	3.318 Ω	85.5 Ω
NPC-600	2.441 Ω	106.4 Ω	3.216 Ω	69.9 Ω
NPC-750	2.231 Ω	76.8 Ω	3.027 Ω	50.5 Ω
NPC-750	2.256 Ω	89.6 Ω	3.309 Ω	60.6 Ω

Fig. 3. (a) Rate performance at current densities between 0.1 A/g and 10 A/g of PC-750 and NPC-Ts. The Nyquist plots of EIS and the fitted data of PC-750 and NPC-Ts of (b) fresh cell and (c) after 5 cycles. (d) The fitted results of EIS. (e) Stability test of NPC-750 for 5000 cycles at 10 A/g.

performance of NPC-750 among NPC-T. The N contents of NPC-600, NPC-750 and NPC-900 were calculated to be 2.23, 2.85 and 1.47 at%, respectively. The N 1s spectra can be fitted to three peaks at ~398.9, ~400.2, ~401.0 eV (Fig. S8c in Supporting information), corresponding to the pyridinic-N, pyrrolic-N and graphitic-N, respectively (Fig. S8d in Supporting information). Apparently, these peaks vary with the calcination temperature, and at the optimal calcination temperature of 750 °C, NPC-750 has the highest pyridinic nitrogen content, resulting in the best Li^+ storage of NPC-750 among NPC-Ts. Moreover, with higher pyridinic-N content, the NPC-600 shows lower Li^+ storage than that of NPC-900 due the important role of SSA and porosity in the Li^+ storage process.

Apart from the excellent cycling stability, the PC-750 and NPC-Ts also exhibit excellent rate capability (Fig. 3a and Table S3 in Supporting information), among NPC-750 obtains the stable and the highest discharge capacities of 989, 687, 375 and 283 mAh/g at 0.1, 1, 5 and 10 A/g, respectively. When the current density goes back to 0.1 A/g, the specific capacity also returns to 1030 mAh/g. Furthermore, to investigate the Li^+ diffusion kinetics, electrochemical impedance spectroscopy (EIS) was performed on the fresh cells aged 12 h and cycled cells after 5 times at 0.1 A/g, and the data are fitted to obtain value of fitted R_s (impedance of electrolyte solution), R_{ct} (charge transfer resistance) and R (total resistance of SEI film and charge transfer resistance) (Figs. 3b-d). Compared with PC-750, NPC-Ts for fresh cells have lower values of R_s, indicating a low charge transfer resistance at the electrolyte/electrode interface, due to the increased surface wettability of PC by N doping. The smallest R_{ct} of 76.8 Ω for NPC-750 indicates the best charge transfer ability. After 5 cycles, R_s of all electrodes increase owing to the formation of SEI films, while the total resistance R decrease, because SEI films is beneficial to Li-ion migration at the interface, and then improves the charge transfer ability [35]. Moreover, the smallest R of NPC-750 also verifies the thin and uniform SEI film, highlighting the excellent Li^+ storge performance of NPC-750. Further, the NPC-750 also exhibits the superior long-term cycling stability at oversize current density of 10 A/g. The initial reversible capacity is 205 mAh/g, then rapidly increases to 281 mAh/g after *ca.* 30 cycles, and the reversible capacity is kept at 219 mAh/g after 5000 cycles (CE *ca.* 100%) (Fig. 3e). It can be obviously observed that the performance, reversibility and practicability of NPC-750 were much superior to that of most the biomass-derived carbon materials and graphene/carbon-based materials (Table S4).

CV curves of NPC-Ts and PC-750 at different scan rates (0.5, 1.0, 1.5, 2 and 5 mV/s) are explored to confirm whether the superior capacity of PC from Agar is contributed by the interfacial Li^+ storage or not. As shown in Figs. S9a and S10–S12 (Supporting information), all CV curves exhibit similar behaviors, and their integral areas increase with the increase of scan rates. According to power law about the measured current (i) and the scan rate (v): $i = av^b$, $0 < b < 0.5$ means Li-ions diffusion process; $0.5 < b < 1$ means the diffusion process and pseudocapacitive behavior together, and $b = 1$ means completely pseudocapacitive behavior control. By calculating, b values amount to 0.7675, 0.8718, 0.8578 and 0.8513 for anodic peak of PC-750, NPC-600, NPC-750 and NPC-900, respectively. These results indicate that the Li-ions storage process is jointly controlled by diffusion and pseudocapacitive behavior in kinetics (Fig. S9b in Supporting information). In addition, the diffusion and capacitive contribution to the current response can be quantitatively examined by the equation: $i = k_1 v + k_2 v^{1/2}$, which the surface capacitance contribution can be obtained through calculating k_1 and k_2 at each potential. As shown in Figs. S9c and d and S10-S12 (Supporting information), the pseudocapacitive con-

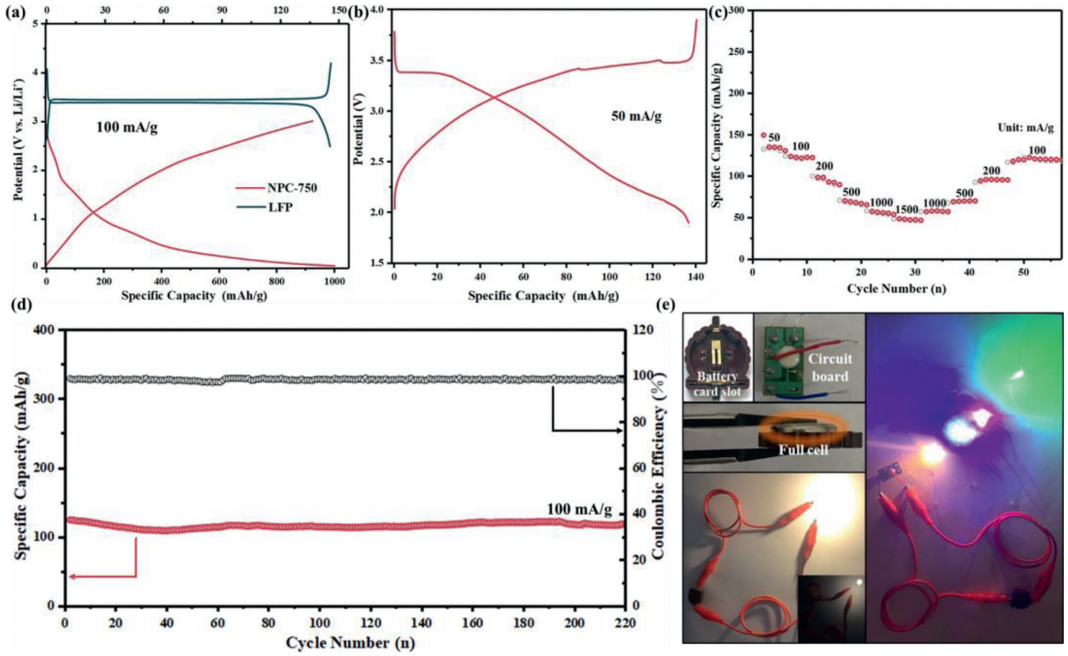

Fig. 4. (a) Charge-discharge voltage profiles of the single electrodes: NPC-750 anode (down curve) at 100 mA/g and the LFP cathode (up curve) at 100 mA/g *versus* Li. (b) Charge-discharge voltage profiles of NPC-750//LFP full cell at 50 mA/g. (c) Rate performance and (d) cycling performance of the full cell between 1.9 V and 3.9 V. (e) Photographs of the button-type full battery and its application in lightening LED.

tribution (red shadow area) is 74.5% of NPC-750 at a scan rate of 5 mV/s, which is higher than that of PC-750 (72.2%), attributed to more interfacial active sites generated by N doping to absorb/store more Li^+. Moreover, NPC-600 (76.6%) is higher than NPC-750 and NPC-900 (70.7%), because the volatilization of N-containing gas results in less interfacial Li^+ storage. Notably, the NPC-750 exhibits the best Li^+ storage performance among all samples, and the Li^+ storage is controlled by synergy of the N doping, pore structure and SSA of PC.

The ultrahigh capacity, excellent cycling stability, and remarkable rate capability of NPC-750 encourage us to further explore its performance in a full cell. A full lithium-ion battery was fabricated using the commercial $LiFePO_4$ (LFP) as cathode and NPC-750 as anode, and the voltage profile of the LFP cathode and NPC-750 anode *versus* Li was shown in Fig. 4a. At a current density of 0.1 A/g, the LFP cathode exhibits a reversible capacity of *ca.* 145 mAh/g and a flat voltage plateau of 3.5 V *versus* Li, while the NPC-750 anode operates reversibly with continuous, plateau-free charge-discharge curves with the capacity of about 1019 mAh/g. On the basis of the half-cell results, the lower and the upper cut-off voltages were set to 1.9 and 3.9 V, respectively, which are highly favorable for practical application. We further evaluated the cycle stability and rate performance of the full cell based on NPC-750 anode. More specifically, the full cell delivers a high reversible capacity of 139 mAh/g and an impressive energy density of 347 Wh/kg at a current rate of 50 mA/g (Fig. 4b), and the good specific capacities of 123.0, 98.8, 69.6 and 56.3 mAh/g at current densities of 100, 200, 500 and 1000 mA/g (Fig. 4c), respectively, indicating the high utilization of NPC-750 (the capacity is calculated based on the total mass of both cathode and anode). Especially, the full cell exhibits a 47.8 mAh/g capacity at 1500 mA/g current density, meaning its remarkable rate performance. When the current density orderly goes back to 1000, 500, 200 and 100 mA/g, the specific capacity returns to 57.8, 70.5, 96.2 and 122.8 mAh/g, respectively. The full cell based on NPC-750 also shows an excellent cycling stability with initial reversible capacity of 125 mAh/g at 100 mA/g (Fig. 4d), which can be kept at 119 mAh/g after 100 cycles. This cell further displays excellent capacity retention of 95% after 220 cycles, much better than most graphene-based or other carbon-based full cells (Table S5 in Supporting information). To demonstrate the practical application of NPC-750, the button-packaged of NPC-750//LFP full cell can drive light-emitting-diodes (LED) coming from commercial children's toys for a long time (Fig. 4e). This result indicates that the low-cost NPC-750 is promising to become a truly commercial anode material for LIBs.

In summary, we successfully prepared low-cost NPC anode materials for LIBs with high cost-performance *via* a facile one-pot pyrolysis of plentiful agar. By delicately regulating the calcination temperature, the obtained NPC-750 as anode materials achieves the best electrochemical performances for the LIBs with a good long-term cycling performance and excellent rate capability (837 mAh/g after 500 cycles at 1 A/g, 219 mAh/g after 5000 cycles at 10 A/g). Remarkably, outstanding practicability can be achieved in a full cell *via* coupling the NPC with $LiFePO_4$ cathode to achieve high capacity and excellent cycling performances (125 mAh/g at 100 mA/g, capacity retention of 95%, after 220 cycles). Such excellent Li^+ storage performance with ultralow cost is extremely rare in reported anode materials of LIBs to date, so the work provides a successfully example about biomass-based PCs as a potentially valuable anode material that can be used as a substitute for graphite.

Declaration of competing interest

The authors declare no competing financial interests.

Acknowledgment

Financial support from the Natural Science Foundation of Shandong Province (No. ZR2021MB025).

References

[1] Y. Zhou, Q. Han, Y. Liu, et al., Energy Storage Mater. 50 (2022) 308–333.
[2] S. Wang, P. Wang, B. Chen, et al., eScience 2 (2022) 339–346.
[3] M.C. Liu, H.J. Chen, G. Wu, et al., Chin. Chem. Lett. 34 (2023) 107546.
[4] S. Li, K. Wang, G. Zhang, et al., Adv. Funct. Mater. 32 (2022) 2200796.

[5] S. Xu, H. Dai, S. Zhu, et al., eScience 1 (2021) 60–68.
[6] D. Zhang, L. Li, W. Zhang, et al., Chin. Chem. Lett. 34 (2023) 107122.
[7] H. Zhang, H. Liu, L.F.J. Piper, et al., Chem. Rev. 122 (2022) 5641–5681.
[8] H. Huang, L. Kong, W. Shuang, et al., Chin. Chem. Lett. 33 (2022) 1037–1041.
[9] T. Hou, B. Liu, X. Sun, et al., ACS Nano 15 (2021) 6735–6746.
[10] N. Zhao, Y. Yang, D. Yi, et al., Chem. Eng. J. 422 (2021) 130018.
[11] Y. Qi, C. Shen, Q. Hou, et al., J. Energy Chem. 72 (2022) 522–531.
[12] H. Liu, W. Yang, S. Che, et al., Carbon 196 (2022) 633–638.
[13] I. Hussain, S. Sahoo, C. Lamiel, et al., Energy Storage Mater. 47 (2022) 13–43.
[14] Y. Mu, M. Han, J. Li, J. Liang, J. Yu, Carbon 173 (2021) 477–484.
[15] W. Deng, Y.L. Wang, W. Guo, et al., Carbon 178 (2021) 573–580.
[16] M. Joe, Y.K. Han, K.R. Lee, et al., Carbon 77 (2014) 1140–1147.
[17] M.S. Balogun, W. Qiu, F. Lyu, et al., Nano Energy 26 (2016) 446–455.
[18] X. Yang, L. Gong, X. Liu, et al., Angew. Chem. Int. Ed. 61 (2022) 202207043.
[19] S. Wang, C. Tang, Y. Huang, J. Gong, Chin. Chem. Lett. 33 (2022) 3802–3808.
[20] W. Long, B. Fang, A. Ignaszak, et al., Chem. Soc. Rev. 46 (2017) 7176–7190.
[21] P. Wang, G. Zhang, X.Y. Wei, et al., J. Am. Chem. Soc. 143 (2021) 3280–3283.
[22] K. Yu, Y. Wang, X. Wang, et al., Mater. Lett. 253 (2019) 405–408.
[23] R. Boonprachai, T. Autthawong, O. Namsar, et al., Crystals 12 (2022) 223.
[24] C. Liao, Y. Hou, L. Han, et al., Carbon 186 (2022) 46–54.
[25] H. Ning, D. Guo, X. Wang, et al., J. Energy Chem. 56 (2021) 113–120.
[26] S. Jeoung, I.T. Ju, J.H. Kim, et al., J. Mater. Chem. A 6 (2018) 18906–18911.
[27] T. Yan, Y. Zou, X. Zhang, et al., ACS Appl. Mater. Interfaces 13 (2021) 9856–9864.
[28] F. Zhang, T. Liu, J. Zhang, et al., Carbon 147 (2019) 451–459.
[29] A. G.Martin, J. M.Fernandez, M. Ruttert, et al., Carbon 164 (2020) 261–271.
[30] J. Lin, Y. Xu, J. Wang, et al., Chem. Eng. J. 352 (2018) 964–971.
[31] J. Niu, R. Shao, M. Liu, et al., Energy Storage Mater. 12 (2018) 145–152.
[32] K. Wang, Y. Xu, H. Wu, et al., Carbon 178 (2021) 443–450.
[33] R.R. Gaddam, D. Yang, R. Narayan, et al., Nano Energy 26 (2016) 346–352.
[34] Y. Huang, K. Li, G. Yang, et al., Small 14 (2018) 1703969.
[35] Z.Y. Wang, W.L. Li, C.F. Pan, Y.H. Sun, J.M. Nan, Appl. Surf. Sci. 587 (2022) 152870.